Synthetic Axion Response with Space-Time Crystals

Filipa R. Prudêncio[1,2,][*] and Mário G. Silveirinha[1]

[1]*University of Lisbon – Instituto Superior Técnico and Instituto de Telecomunicações, Avenida Rovisco Pais 1,
1049-001 Lisbon, Portugal*

[2]*Instituto Universitário de Lisboa (ISCTE-IUL), Avenida das Forças Armadas 376, 1600-077 Lisbon, Portugal*

Here, we show that space-time modulations provide an exciting route to realize complex nonreciprocal couplings, and, in particular, the elusive axion response. We develop an analytical formalism to homogenize anisotropic space-time crystals in the long wavelength limit. It is found that space-time crystals with suitable glide-rotation symmetry can have a giant axion-type response, several orders of magnitude larger than in natural materials. The nonreciprocal axion response may have interesting applications in optics, for example, in electromagnetic isolation, and in addition may enable exciting forms of light-wave interactions.

I. INTRODUCTION

With the rise of metamaterials, the "toolbox" of available electromagnetic responses was greatly expanded in the past two decades. Today, the principles that guide the design of media with rather exotic properties, e.g., a double negative permittivity and permeability [1], extreme anisotropy [2], hyperbolic isofrequency contours [3,4], topological systems immune to backscattering relying on a duality symmetry [5–7], and others, are well understood. There is however a rather peculiar class of materials for which limited progress has been achieved. That is the class of media with an axion or Tellegen coupling [8–12]. In its simpler isotropic version, such materials are characterized by a constitutive relation of the form:

$$\mathbf{D} = \varepsilon_0 \varepsilon \mathbf{E} + \frac{\kappa}{c} \mathbf{H}, \ \mathbf{B} = \frac{\kappa}{c} \mathbf{E} + \mu_0 \mu \mathbf{H} \qquad (1)$$

where κ is the Tellegen parameter. Here, **E** is the electric field, **H** is the magnetic field, **D** is the electric displacement, and **B** is the magnetic induction field. The axion medium is nonreciprocal, but different from typical nonreciprocal gyrotropic materials (e.g., ferrites and other iron garnets), the nonreciprocity does not necessarily require an external bias and may be anchored in a spontaneous time-symmetry breaking [11], e.g., due to antiferromagnetism [12–14].

Remarkably the electromagnetic response of an isotropic Tellegen medium can be linked through a duality transformation to the response of conventional dielectrics [9,15]. Therefore, the dispersion of waves in Tellegen materials

is in some cases indistinguishable from the dispersion in conventional structures [9,10,12]. This property has led to some scientific debate on the physical viability of the axion response [16–22]. Today, this debate is settled, and it is widely accepted that axion-type responses can emerge spontaneously—albeit extremely weak—in nature in some antiferromagnetic materials [13], and most notably in electronic topological insulators [14,23–25]. Furthermore, the elusive axion response is interesting also from a conceptual point of view due to its connections with high-energy physics. It was suggested by Wilczek that "axions" may provide an explanation for dark matter [26].

As mentioned previously, the Tellegen parameter κ of naturally available materials is usually negligibly small. For example, for Cr_2O_3 it is on the order of 10^{-4} [13]. Due to this reason, the signature of Tellegen-induced electromagnetic phenomena is rather faint, and can be ignored for all practical purposes. Tellegen materials can be, in principle, synthesized artificially. A proposal relying on a gyrotropic magnetic particle is reported in Ref. [27]. A related idea relying on an electrically biased gyrotropic particle [28] is described in Ref. [29].

Recently, the time modulation of the material parameters has opened up opportunities in the design of different classes of metamaterials [30–39]. For example, since the time modulation breaks the Lorentz reciprocity in electromagnetism, it has been shown that time-varying material responses can be used to realize unidirectional guides and isolators, multifunctional nonreciprocal metasurfaces, and others, without an external magnetic bias [30–37]. Moreover, rather remarkably, time-modulated photonic crystals can be used as a platform to synthesize exotic metamaterial responses [40–43]. In particular, it was shown in

---

024031-1

Ref. [43] that space-time crystals with a traveling wave-type space-time modulation behave in many ways as a synthetic moving medium. In such systems the permittivity and permeability depend on the space-time coordinates as $\varepsilon = \varepsilon(z - vt)$ and $\mu = \mu(z - vt)$, with v the modulation speed. This type of modulation leads to a synthetic Fresnel drag effect such that the electromagnetic waves are dragged by the synthetic motion of the medium, in the same manner as they would be dragged by a moving material body [41]. Moreover, in the long wavelength limit, the space-time crystal can be described using effective parameters, which reproduce the well-known moving medium coupling [41,43,44]. The velocity of the equivalent moving medium is different from the modulation velocity v, and, curiously, its sign may also differ from the sign of v.

In view of these developments, it is natural to wonder if it may be possible to implement the axion coupling using a space-time modulated crystal. Here, using homogenization theory and full-wave simulations, we demonstrate that, indeed, space-time modulated systems offer a unique opportunity to realize a metamaterial with a giant axion-type response.

The paper is organized as follows. In Sec. II, we extend the homogenization theory of Ref. [43] to anisotropic space-time crystals with a traveling wave-type space-time modulation. Based on symmetry considerations, we propose a general solution to design an effective medium that behaves as a moving-Tellegen medium for propagation along the direction of the modulation velocity. In particular, we present a simple solution to implement the synthetic axion response. In Sec. III, we present a detailed study of the effective response of the synthetic axion material. In addition, we illustrate the impact of the synthetic axion coupling by studying the reflection of a plane wave at an interface between air and the effective material. It is shown that the space-time modulation can result in a giant rotation of polarization of the incident wave. Finally, Sec. IV summarizes the main conclusions.

II. HOMOGENIZATION OF ANISOTROPIC SPACE-TIME SYSTEMS

We consider a generic one-dimensional space-time crystal with constitutive relations of the type

$$\mathbf{D}(x,y,z,t) = \varepsilon_0 \bar{\varepsilon}(z - vt) \cdot \mathbf{E}(x,y,z,t),$$
$$\mathbf{B}(x,y,z,t) = \mu_0 \bar{\mu}(z - vt) \cdot \mathbf{H}(x,y,z,t). \quad (2)$$

The material parameters vary both in space and in time, but are constant for space-time points such that $z' = z - vt = $ const., v being the modulation speed. This is known as a traveling wave modulation, and different aspects of it have been studied by several authors in recent years [34,35,41–43] (for earlier works see Refs. [45,46]). Here, we suppose that the permittivity and the permeability

are anisotropic and described by real-valued symmetric periodic tensors of the type:

$$\bar{\varepsilon} = \begin{pmatrix} \varepsilon_{xx} & \varepsilon_{xy} & 0 \\ \varepsilon_{xy} & \varepsilon_{yy} & 0 \\ 0 & 0 & \varepsilon_{zz} \end{pmatrix}, \quad \bar{\mu} = \begin{pmatrix} \mu_{xx} & \mu_{xy} & 0 \\ \mu_{xy} & \mu_{yy} & 0 \\ 0 & 0 & \mu_{zz} \end{pmatrix}, \quad (3)$$

with $\bar{\varepsilon}(z') = \bar{\varepsilon}(z' + a)$ and $\bar{\mu}(z') = \bar{\mu}(z' + a)$ periodic functions with a spatial period a (see Fig. 1). Time-dependent anisotropic materials can enable rather peculiar electromagnetic phenomena [47,48].

Due to the assumed structure of $\bar{\varepsilon}$ and $\bar{\mu}$ [Eq. (3)], the directions that diagonalize each of the tensors (loosely referred to "optical axes") are such that (i) two optical axes are in the x-o-y plane and (ii) the third optical axis is along z. Recently, it has been shown that by changing continuously the optical axes it is possible to realize an Archimedes screw for light [42]. In contrast, in the present work the optical axes are fixed, i.e., independent of space and time. However, the permittivity and permeability tensors in general may not share the same optical axes in the x-o-y plane [see Fig. 2(a)]. The angular offset between the permeability and permittivity optical axes is denoted by θ. It is shown in Sec. III that a nontrivial θ is the key to unlock the axion response.

For future reference, we introduce a 4×4 matrix that describes the transverse material response of the space-time crystal:

$$\mathbf{M}_\perp(z') = \begin{pmatrix} \varepsilon_0 \bar{\varepsilon}_\perp & \mathbf{0}_{2\times 2} \\ \mathbf{0}_{2\times 2} & \mu_0 \bar{\mu}_\perp \end{pmatrix}, \text{ with} \quad (4a)$$

$$\bar{\varepsilon}_\perp = \begin{pmatrix} \varepsilon_{xx}(z') & \varepsilon_{xy}(z') \\ \varepsilon_{xy}(z') & \varepsilon_{yy}(z') \end{pmatrix}, \text{ and} \quad (4b)$$

$$\bar{\mu}_\perp = \begin{pmatrix} \mu_{xx}(z') & \mu_{xy}(z') \\ \mu_{xy}(z') & \mu_{yy}(z') \end{pmatrix}.$$

A. General homogenization theory

The homogenization of the space-time crystal is done using the same strategy as in Ref. [43]. First, we use a Galilean coordinate transformation ($\mathbf{r}' = \mathbf{r} - \mathbf{v}t, t' = t$) to switch to a frame (the "co-moving frame") where the material parameters become independent of time. Then, the crystal response is homogenized in the co-moving frame. Finally, we use the inverse Galilean transformation to determine the effective response in the original "laboratory" frame.
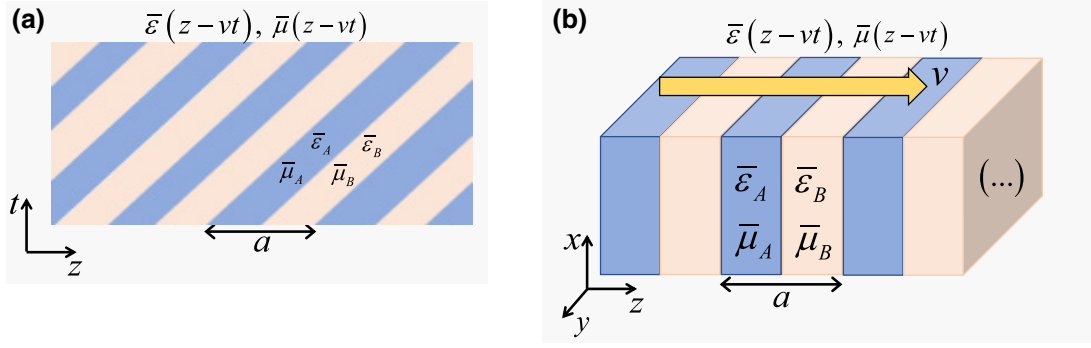
FIG. 1. Anisotropic space-time crystal formed by two layers with material tensors $\bar{\varepsilon}_A, \bar{\mu}_A$ and $\bar{\varepsilon}_B, \bar{\mu}_B$. (a) Representation of the material parameters in a space-time diagram. (b) Sketch of the stratified crystal in real space with the arrow indicating how the material parameters vary in time. The modulation speed is $\mathbf{v} = v\hat{\mathbf{z}}$.

To begin with, we write Maxwell's equations in the lab frame in the following compact manner:

$$\underbrace{\begin{pmatrix} \mathbf{0} & i\nabla \times \mathbf{1}_{3\times3} \\ -i\nabla \times \mathbf{1}_{3\times3} & \mathbf{0} \end{pmatrix}}_{\hat{N}(-i\nabla)} \cdot \begin{pmatrix} \mathbf{E} \\ \mathbf{H} \end{pmatrix} = i\frac{\partial}{\partial t}\begin{pmatrix} \mathbf{D} \\ \mathbf{B} \end{pmatrix}, \quad (5a)$$

$$\begin{pmatrix} \mathbf{D} \\ \mathbf{B} \end{pmatrix} = \begin{pmatrix} \bar{\varepsilon}(z - v_0 t) & \mathbf{0} \\ \mathbf{0} & \bar{\mu}(z - v_0 t) \end{pmatrix} \cdot \begin{pmatrix} \mathbf{E} \\ \mathbf{H} \end{pmatrix}$$

$$\equiv \mathbf{M}(z - v_0 t) \cdot \begin{pmatrix} \mathbf{E} \\ \mathbf{H} \end{pmatrix}. \quad (5b)$$

The structure of the above equations is preserved under a Galilean transformation (or more generally under a Lorentz transformation). Therefore, the fields in the co-moving frame satisfy $\hat{N}(-i\nabla') \cdot \begin{pmatrix} \mathbf{E}' \\ \mathbf{H}' \end{pmatrix} = i(\partial/\partial t)\begin{pmatrix} \mathbf{D}' \\ \mathbf{B}' \end{pmatrix}$ with $\begin{pmatrix} \mathbf{D}' \\ \mathbf{B}' \end{pmatrix} = \mathbf{M}'(z') \cdot \begin{pmatrix} \mathbf{E}' \\ \mathbf{H}' \end{pmatrix}$. Here, $\mathbf{M}'(z')$ is the (time-independent) material matrix in the co-moving frame,

which is related to the unprimed material matrix as [see Appendix A, Eq. (A8)]:

$$\mathbf{M}' = \mathbf{M} \cdot [\mathbf{1}_{6\times6} + \mathbf{V} \cdot \mathbf{M}]^{-1}, \quad \text{with}$$

$$\mathbf{V} = \begin{pmatrix} \mathbf{0}_{3\times3} & \mathbf{v} \times \mathbf{1}_{3\times3} \\ -\mathbf{v} \times \mathbf{1}_{3\times3} & \mathbf{0}_{3\times3} \end{pmatrix}. \quad (6)$$

In the above, $\mathbf{v} = v\hat{\mathbf{z}}$ is the modulation speed.

It is shown in Appendix B that the standard homogenization approach for stratified structures can be readily generalized to anisotropic space-time crystals. The effective material matrix in the lab frame $\mathbf{M}_{\text{ef}}$ links the spatially averaged fields as follows: $\begin{pmatrix} \langle\mathbf{D}\rangle \\ \langle\mathbf{B}\rangle \end{pmatrix} = \mathbf{M}_{\text{ef}} \cdot \begin{pmatrix} \langle\mathbf{E}\rangle \\ \langle\mathbf{H}\rangle \end{pmatrix}$. For "microscopic" electric and magnetic responses as in Eq. (3), the effective material response is such that

$$\mathbf{M}_{\text{ef}} = \begin{pmatrix} \varepsilon_0\overline{\varepsilon_{\text{ef}}} & \frac{1}{c}\overline{\xi_{\text{ef}}} \\ \frac{1}{c}\overline{\zeta_{\text{ef}}} & \mu_0\overline{\mu_{\text{ef}}} \end{pmatrix}, \quad \text{with} \quad (7a)$$
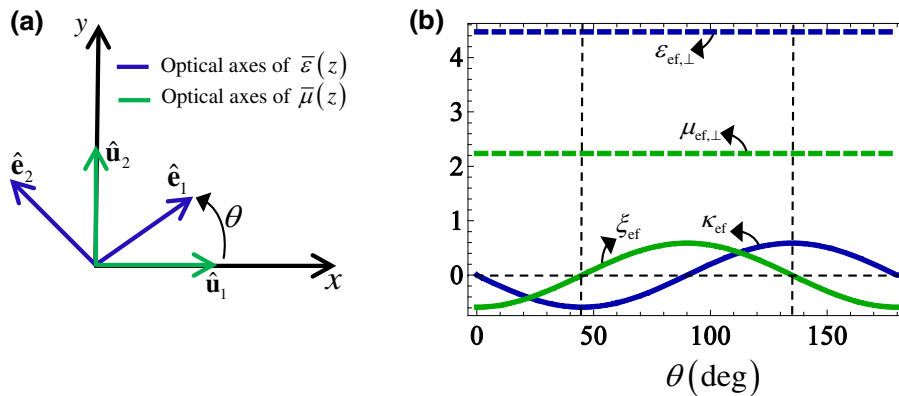

FIG. 2. (a) Optical axes of the permittivity and permeability tensors, $\bar{\varepsilon}(z)$ and $\bar{\mu}(z)$, respectively. The offset angle is denoted by θ. (b) Parameters of the effective moving-Tellegen medium, $\varepsilon_{\text{ef},\perp}, \mu_{\text{ef},\perp}, \kappa_{\text{ef}}, \xi_{\text{ef}}$, as a function of the angle θ, for $\varepsilon_1 = 6$, $\varepsilon_2 = 2$, $\mu_1 = 3$ and $\mu_2 = 1$. An effective moving medium is obtained for $\theta = 0, 90°, 180°$, whereas for $\theta = 45°, 135°$ (dashed vertical grid lines) a pure axion response is achieved. The modulation speed is $v = 0.2c$.

$$\overline{\varepsilon_{\text{ef}}} = \begin{pmatrix} \varepsilon_{\text{ef},xx} & \varepsilon_{\text{ef},xy} & 0 \\ \varepsilon_{\text{ef},xy} & \varepsilon_{\text{ef},yy} & 0 \\ 0 & 0 & \varepsilon_{\text{ef},zz} \end{pmatrix},$$

$$\overline{\mu_{\text{ef}}} = \begin{pmatrix} \mu_{\text{ef},xx} & \mu_{\text{ef},xy} & 0 \\ \mu_{\text{ef},xy} & \mu_{\text{ef},yy} & 0 \\ 0 & 0 & \mu_{\text{ef},zz} \end{pmatrix}, \quad (7\text{b})$$

$$\overline{\xi_{\text{ef}}} = \overline{\zeta_{\text{ef}}}^T = \begin{pmatrix} \xi_{\text{ef},xx} & \xi_{\text{ef},xy} & 0 \\ \xi_{\text{ef},yx} & \xi_{\text{ef},yy} & 0 \\ 0 & 0 & 0 \end{pmatrix}. \quad (7\text{c})$$

The general formula for the effective material parameters is given in Appendix B [Eqs. (B4) and (B5)]. The effective parameters $\varepsilon_{\text{ef},zz}$ and $\mu_{\text{ef},zz}$ can be expressed in terms of $\varepsilon_{zz}(z')$ and $\mu_{zz}(z')$ as

$$\varepsilon_{\text{ef},zz} = \left[\frac{1}{a} \int_0^a \frac{1}{\varepsilon_{zz}(z')} dz' \right]^{-1} \text{ and}$$

$$\mu_{\text{ef},zz} = \left[\frac{1}{a} \int_0^a \frac{1}{\mu_{zz}(z')} dz' \right]^{-1}. \quad (8)$$

Note that $\varepsilon_{\text{ef},zz}$ and $\mu_{\text{ef},zz}$ are independent of the modulation speed. Indeed, in the long wavelength limit, the response of the crystal along the z direction (parallel to the modulation speed) is effectively decoupled from the response of the material in the x-o-y plane (see Appendix A).

Since the response in the x-o-y plane is decoupled from the response along the z direction, it is possible to write the remaining effective parameters in terms of $\mathbf{M}_\perp$ [Eq. (4)]. To this end, it is convenient to introduce the 4×4 matrix

$$\mathbf{M}_{\text{ef},\perp} = \begin{pmatrix} \varepsilon_0 \bar{\varepsilon}_{\text{ef},\perp} & \frac{1}{c} \bar{\xi}_{\text{ef},\perp} \\ \frac{1}{c} \bar{\zeta}_{\text{ef},\perp} & \mu_0 \bar{\mu}_{\text{ef},\perp} \end{pmatrix}, \quad (9)$$

where $\bar{\varepsilon}_{\text{ef},\perp} \equiv \begin{pmatrix} \varepsilon_{\text{ef},xx} & \varepsilon_{\text{ef},xy} \\ \varepsilon_{\text{ef},xy} & \varepsilon_{\text{ef},yy} \end{pmatrix}$, $\overline{\mu}_{\text{ef},\perp} \equiv \begin{pmatrix} \mu_{\text{ef},xx} & \mu_{\text{ef},xy} \\ \mu_{\text{ef},xy} & \mu_{\text{ef},yy} \end{pmatrix}$, and $\overline{\xi}_{\text{ef},\perp} = (\overline{\zeta}_{\text{ef},\perp})^T \equiv \begin{pmatrix} \xi_{\text{ef},xx} & \xi_{\text{ef},xy} \\ \xi_{\text{ef},yx} & \xi_{\text{ef},yy} \end{pmatrix}$ are 2×2 matrices that determine the effective response of the space-time

crystal in the x-o-y plane [Eq. (7)]. Using Eqs. (B4) and (B5) one may show that

$$\mathbf{M}_{\text{ef},\perp} = \mathbf{M}'_{\text{ef},\perp} \cdot [\mathbf{1}_{4\times4} - v\boldsymbol{\sigma} \cdot \mathbf{M}'_{\text{ef},\perp}]^{-1}, \text{ with} \quad (10\text{a})$$

$$\mathbf{M}'_{\text{ef},\perp} = \frac{1}{a} \int_0^a dz' \mathbf{M}_\perp(z') \cdot [\mathbf{1}_{4\times4} + v\boldsymbol{\sigma} \cdot \mathbf{M}_\perp(z')]^{-1}, \quad (10\text{b})$$

$$\boldsymbol{\sigma} = \begin{pmatrix} \mathbf{0}_{2\times2} & \mathbf{J} \\ -\mathbf{J} & \mathbf{0}_{2\times2} \end{pmatrix}, \text{ with } \mathbf{J} = \begin{pmatrix} 0 & -1 \\ 1 & 0 \end{pmatrix}. \quad (10\text{c})$$

Note that $\mathbf{M}_{\text{ef},\perp}, \mathbf{M}'_{\text{ef},\perp}, \mathbf{M}_\perp, \boldsymbol{\sigma}$ are all 4×4 real-valued matrices. In general, the effective response in the lab frame is bianisotropic so that the magnetoelectric tensors $\overline{\xi}_{\text{ef}}, \overline{\zeta}_{\text{ef}}$ are nontrivial. Analogous to Ref. [43], it can be shown that a nontrivial bianisotropic response can occur only when both the permittivity and permeability tensors are simultaneously modulated in space and in time.

B. Glide-rotation symmetry

Next, we show that by enforcing the invariance of the space-time crystal under a particular glide symmetry, it is possible to reduce drastically the complexity of the effective response. The glide symmetry ensures that the material response is invariant under continuous rotations about the z axis, i.e., independent of the field polarization in the x-o-y plane.

It is convenient to write the transverse permittivity and permeability tensors [Eq. (4)] as a function of its eigenvalues. As shown in Fig. 2(a), it is supposed without loss of generality that the principal axes of the permeability are aligned with the x and y directions: $\hat{\mathbf{u}}_1 \equiv \hat{\mathbf{x}}$, $\hat{\mathbf{u}}_2 \equiv \hat{\mathbf{y}}$. The principal axes of the permittivity tensor $\hat{\mathbf{e}}_1, \hat{\mathbf{e}}_2$ are tilted by θ with respect to the axes of the permeability. These properties imply that $\overline{\mu}_\perp(z,t) = \mu_1(z')\hat{\mathbf{u}}_1 \otimes \hat{\mathbf{u}}_1 + \mu_2(z')\hat{\mathbf{u}}_2 \otimes \hat{\mathbf{u}}_2$ and $\bar{\varepsilon}_\perp(z,t) = \varepsilon_1(z')\hat{\mathbf{e}}_1 \otimes \hat{\mathbf{e}}_1 + \varepsilon_2(z')\hat{\mathbf{e}}_2 \otimes \hat{\mathbf{e}}_2$ with $z' = z - vt$ and μ_1, μ_2 ($\varepsilon_1, \varepsilon_2$) the eigenvalues of the permeability (permittivity). The two tensors can be explicitly written in the x-o-y coordinate system as

$$\bar{\varepsilon}_\perp(z,t) = \begin{pmatrix} \varepsilon_1(z')\cos^2\theta + \varepsilon_2(z')\sin^2\theta & [\varepsilon_1(z') - \varepsilon_2(z')]\cos\theta\sin\theta \\ [\varepsilon_1(z') - \varepsilon_2(z')]\cos\theta\sin\theta & \varepsilon_1(z')\sin^2\theta + \varepsilon_2(z')\cos^2\theta \end{pmatrix}, \quad (11\text{a})$$

$$\overline{\mu}_\perp(z,t) = \begin{pmatrix} \mu_1(z') & 0 \\ 0 & \mu_2(z') \end{pmatrix}. \quad (11\text{b})$$

Let us now suppose that eigenvalues of each material tensor are linked as follows:

$$\varepsilon_2(z') = \varepsilon_1\left(z' - \frac{a}{2}\right), \quad \mu_2(z') = \mu_1\left(z' - \frac{a}{2}\right). \quad (12)$$

In such a case, the microscopic (transverse) material matrix $\mathbf{M}_\perp$ [Eq. (4a)] is invariant under a rotation of 90° about the z axis followed by a translation by half lattice constant:

$$\mathbf{M}_\perp(z') = \begin{pmatrix} \mathbf{J}^T & \mathbf{0}_{2\times2} \\ \mathbf{0}_{2\times2} & \mathbf{J}^T \end{pmatrix} \cdot \mathbf{M}_\perp\left(z' - \frac{a}{2}\right) \cdot \begin{pmatrix} \mathbf{J} & \mathbf{0}_{2\times2} \\ \mathbf{0}_{2\times2} & \mathbf{J} \end{pmatrix}, \tag{13}$$

with the 90°-rotation matrix introduced in Sec. III A. We refer to this transformation symmetry as a *glide-rotation symmetry* (see Ref. [49] for an overview of glide symmetries). Evidently, the effective medium theory must preserve the glide-rotation symmetry. As the homogenized response is independent of the space-time coordinates, it follows that

$$\mathbf{M}_{\perp,\text{ef}} = \begin{pmatrix} \mathbf{J}^T & \mathbf{0}_{2\times2} \\ \mathbf{0}_{2\times2} & \mathbf{J}^T \end{pmatrix} \cdot \mathbf{M}_{\perp,\text{ef}} \cdot \begin{pmatrix} \mathbf{J} & \mathbf{0}_{2\times2} \\ \mathbf{0}_{2\times2} & \mathbf{J} \end{pmatrix}. \tag{14}$$

Substituting now Eq. (9) into the above formula, it is found that the enforced symmetry implies that $\bar{\varepsilon}_{\text{ef},\perp} = \mathbf{J}^T \cdot \bar{\varepsilon}_{\text{ef},\perp} \cdot \mathbf{J}$, $\bar{\mu}_{\text{ef},\perp} = \mathbf{J}^T \cdot \bar{\mu}_{\text{ef},\perp} \cdot \mathbf{J}$, and $\bar{\xi}_{\text{ef},\perp} = \mathbf{J}^T \cdot \bar{\xi}_{\text{ef},\perp} \cdot \mathbf{J}$. Since $\bar{\varepsilon}_{\text{ef},\perp}, \bar{\mu}_{\text{ef},\perp}$ are symmetric tensors they must be scalars: $\bar{\varepsilon}_{\text{ef},\perp} = \varepsilon_{\text{ef},\perp}\mathbf{1}_\perp$ and $\bar{\mu}_{\text{ef},\perp} = \mu_{\text{ef},\perp}\mathbf{1}_\perp$. On the other hand, the magnetoelectric tensors are determined by two scalar parameters $\kappa_{\text{ef}}, \xi_{\text{ef}}$ such that $\bar{\xi}_{\text{ef},\perp} = \kappa_{\text{ef}}\mathbf{1}_\perp - \xi_{\text{ef}}\mathbf{J}$ and $\bar{\zeta}_{\text{ef},\perp} = (\bar{\xi}_{\text{ef},\perp})^T = \kappa_{\text{ef}}\mathbf{1}_\perp + \xi_{\text{ef}}\mathbf{J}$. Note that $\kappa_{\text{ef}} = \xi_{xx,\text{ef}} = \xi_{yy,\text{ef}}$ and $\xi_{\text{ef}} = \xi_{xy,\text{ef}} = -\xi_{yx,\text{ef}}$. Furthermore, the global effective material response [Eq. (7a)] is described by tensors such that

$$\overline{\overline{\varepsilon}}_{\text{ef}} = \varepsilon_{\text{ef},\perp}(\hat{\mathbf{x}}\otimes\hat{\mathbf{x}} + \hat{\mathbf{y}}\otimes\hat{\mathbf{y}}) + \varepsilon_{\text{ef}zz}\hat{\mathbf{z}}\otimes\hat{\mathbf{z}}, \tag{15a}$$

$$\overline{\overline{\mu}}_{\text{ef}} = \mu_{\text{ef},\perp}(\hat{\mathbf{x}}\otimes\hat{\mathbf{x}} + \hat{\mathbf{y}}\otimes\hat{\mathbf{y}}) + \mu_{\text{ef}zz}\hat{\mathbf{z}}\otimes\hat{\mathbf{z}}, \tag{15b}$$

$$\overline{\overline{\xi}}_{\text{ef}} = (\overline{\overline{\zeta}}_{\text{ef},\perp})^T = \kappa_{\text{ef}}(\hat{\mathbf{x}}\otimes\hat{\mathbf{x}} + \hat{\mathbf{y}}\otimes\hat{\mathbf{y}}) - \xi_{\text{ef}}\hat{\mathbf{z}}\times\mathbf{1}. \tag{15c}$$

The above equations show that the homogenized material response is invariant under arbitrary rotations about the z axis. Clearly, the effective material matrix $\mathbf{M}_{\text{ef}}$ is always symmetric and real valued and thereby the response is Hermitian in the long wavelength limit. Evidently, the first piece of the magnetoelectric tensors is a symmetric tensor that provides the axion (Tellegen) piece [50]. The axion response is isotropic in the x-o-y plane, and vanishes along the z direction. On the other hand, the second term of $\overline{\overline{\xi}}_{\text{ef}}$ provides an antisymmetric moving-medium piece [50]. Both terms originate nonreciprocity in the long wavelength limit. A material with $\kappa_{\text{ef}} \neq 0$ and $\xi_{\text{ef}} \neq 0$ is known as a moving-Tellegen medium. In the next subsection, we provide explicit formulas for all the effective parameters for a two-phase system and show how by tuning the angle θ it is possible to control the relative strength of κ_{ef} and ξ_{ef}.

In summary, the glide-rotation symmetry [Eq. (12)] ensures that the effective response is independent of the field polarization in the x-o-y plane (see also the next subsection), and that the global response is coincident with that of a moving-Tellegen medium.

C. Two-phase space-time crystal

The glide-rotation symmetry constraint [Eq. (12)] can be implemented with a two-phase crystal such that the unit cell is formed by two layers A and B of identical thickness $d = a/2$ (see Fig. 1). The layer B is identical to layer A apart from a 90° rotation about the z axis. This means that $\bar{\varepsilon}_{\perp,B} = \mathbf{J}^T \cdot \bar{\varepsilon}_{\perp,A} \cdot \mathbf{J}$ and $\bar{\mu}_{\perp,B} = \mathbf{J}^T \cdot \bar{\mu}_{\perp,A} \cdot \mathbf{J}$. These formulas can be written explicitly as a function of the permittivity and permeability components in the x-o-y coordinate system

$$\begin{pmatrix} \varepsilon_{11} & \varepsilon_{12} \\ \varepsilon_{12} & \varepsilon_{22} \end{pmatrix}_{\text{mat. }A} = \begin{pmatrix} \varepsilon_{22} & -\varepsilon_{12} \\ -\varepsilon_{12} & \varepsilon_{11} \end{pmatrix}_{\text{mat. }B},$$

$$\begin{pmatrix} \mu_{11} & \mu_{12} \\ \mu_{12} & \mu_{22} \end{pmatrix}_{\text{mat. }A} = \begin{pmatrix} \mu_{22} & -\mu_{12} \\ -\mu_{12} & \mu_{11} \end{pmatrix}_{\text{mat. }B}, \tag{16}$$

where the subscripts "mat. A" and "mat. B" indicate if the permittivity and permeability components are calculated for material A or for material B, respectively. Clearly, the material parameters of layer A determine the entire geometry of the space-time crystal.

Substituting the above material parameters in Eq. (10) one obtains after some manipulations the following analytical expressions for the effective parameters of the resulting a moving Tellegen bianisotropic material:

$$\varepsilon_{\text{ef},\perp} = \frac{\varepsilon_{11} + \varepsilon_{22} - (\varepsilon_{11}\varepsilon_{22} - \varepsilon_{12}^2)(\mu_{11} + \mu_{22})v^2}{2 - (1/2)(\varepsilon_{11} + \varepsilon_{22})(\mu_{11} + \mu_{22})v^2},$$

$$\mu_{\text{ef},\perp} = \frac{\mu_{11} + \mu_{22} - (\mu_{11}\mu_{22} - \mu_{12}^2)(\varepsilon_{11} + \varepsilon_{22})v^2}{2 - (1/2)(\varepsilon_{11} + \varepsilon_{22})(\mu_{11} + \mu_{22})v^2} \tag{17a}$$

$$\kappa_{\text{ef}} = v\frac{(\varepsilon_{11} - \varepsilon_{22})\mu_{12} - (\mu_{11} - \mu_{22})\varepsilon_{12}}{2 - (1/2)(\varepsilon_{11} + \varepsilon_{22})(\mu_{11} + \mu_{22})v^2} \text{ and}$$

$$\xi_{\text{ef}} = -v\frac{(1/2)(\varepsilon_{11} - \varepsilon_{22})(\mu_{11} - \mu_{22}) + 2\varepsilon_{12}\mu_{12}}{2 - (1/2)(\varepsilon_{11} + \varepsilon_{22})(\mu_{11} + \mu_{22})v^2}. \tag{17b}$$

In the above formulas, all the permittivity and permeability elements are evaluated for layer A. Using Eq. (11) the effective parameters can also be written in terms of the eigenvalues of the permittivity and permeability tensors
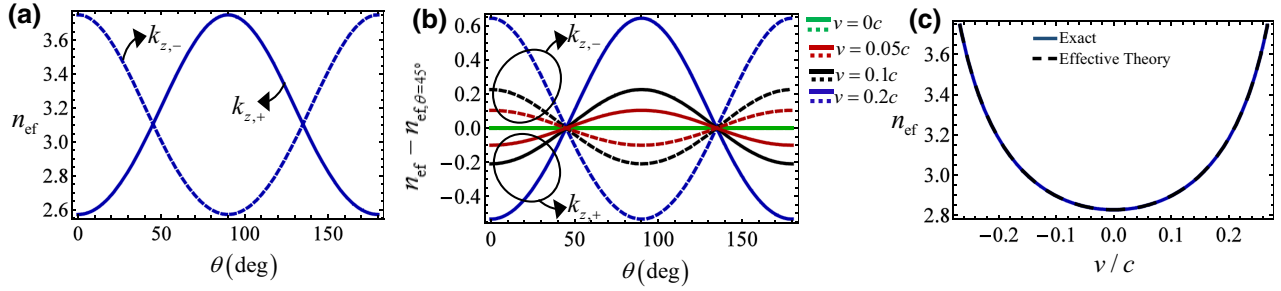
FIG. 3. (a) Refractive index n_{ef} seen by the waves propagating along the $+z$ direction (solid line) and by the waves propagating along the $-z$ direction (dashed line) as a function of the angle θ, for $\varepsilon_1 = 6$, $\varepsilon_2 = 2$, $\mu_1 = 3$, and $\mu_2 = 1$, and modulation speed $v = 0.2c$. (b) Similar to (a) but for different modulation speeds. The vertical axis gives the shift of n_{ef} with respect to n_{ef} calculated for $\theta = 45°$. (c) Equivalent refractive index n_{ef} of an effective axion medium ($\theta = 45°$) as a function of the modulation speed v calculated with (i) the slopes of the exact dispersion diagram of the space-time crystal in the long wavelength limit (solid line), and (ii) the effective medium theory (dashed line).

and of the θ angle as follows:

$$\varepsilon_{ef,\perp} = \frac{\varepsilon_1 + \varepsilon_2 - \varepsilon_1\varepsilon_2(\mu_1 + \mu_2)v^2}{2 - (1/2)(\varepsilon_1 + \varepsilon_2)(\mu_1 + \mu_2)v^2},$$

$$\mu_{ef,\perp} = \frac{\mu_1 + \mu_2 - \mu_1\mu_2(\varepsilon_1 + \varepsilon_2)v^2}{2 - (1/2)(\varepsilon_1 + \varepsilon_2)(\mu_1 + \mu_2)v^2}. \quad (18a)$$

$$\kappa_{ef} = -\frac{v}{2}\frac{(\varepsilon_1 - \varepsilon_2)(\mu_1 - \mu_2)\sin 2\theta}{2 - (1/2)(\varepsilon_1 + \varepsilon_2)(\mu_1 + \mu_2)v^2} \quad \text{and}$$

$$\xi_{ef} = -\frac{v}{2}\frac{(\varepsilon_1 - \varepsilon_2)(\mu_1 - \mu_2)\cos 2\theta}{2 - (1/2)(\varepsilon_1 + \varepsilon_2)(\mu_1 + \mu_2)v^2}. \quad (18b)$$

Again, the eigenvalues of the permittivity and of the permeability are evaluated for layer A. Interestingly, the transverse effective permittivity and permeability are independent of the angle θ. Furthermore, $\kappa_{ef}^2 + \xi_{ef}^2$ is also independent of θ. However, the relative strength of the axion and moving couplings is evidently controlled by the angle 2θ.

Figure 2(b) shows the effective parameters $\varepsilon_{ef,\perp}, \mu_{ef,\perp}, \kappa_{ef}, \xi_{ef}$ as a function of θ, for a modulation speed $v = 0.2c$ in the subluminal regime. We choose a high contrast between the permittivity and permeability eigenvalues to make more evident the impact of the space-time modulation. As seen, when the optical axes of the permittivity and permeability tensors are aligned, i.e., $\theta = 0, 90°, 180°$ the axion parameter vanishes, $\kappa_{ef} = 0$, resulting in an effective moving medium [41,43,44]. On the other hand, in agreement with Eq. (18b), it is possible to obtain a pure axion response by choosing $\theta = 45°, 135°$ so that $\xi_{ef} = 0$.

Figure 3(a) depicts the refractive index seen by the waves propagating along the $+z$ direction (solid line) and by the waves propagating along the $-z$ direction (dashed line) as a function of the angle θ. Due to the invariance of the response under continuous rotations about the z axis, the refractive index is independent of the wave polarization

for all θ. However, the refractive indices of counterpropagating waves are typically different, originating thereby a synthetic Fresnel drag in agreement with earlier works [41,43]. Interestingly, for a pure axion ($\theta = 45°, 135°$) the refractive indices become identical and there is no Fresnel drag. The difference between the two refractive indices is maximized for $\theta = 0°, 90°$, which correspond to an ideal synthetic moving medium ($\kappa_{ef} = 0$). Figure 3(b) shows a study similar to that of Fig. 3(a), but for different modulation speeds. As seen, the asymmetry between the two refractive indices is enhanced for larger values of v.

The refractive indices depicted in Figs. 3(a) and 3(b) are determined using the homogenization theory [Eq. (18)]. Notably, the homogenization result agrees exactly with the result obtained from the slopes of the dispersion of the Bloch modes of the space-time crystal near the point ($\omega = 0, k_z = 0$) (see Appendix C). This property is illustrated in Fig. 3(c) for the particular case of a pure axion response ($\theta = 45°$) and is further discussed in Sec. III.

In summary, the key ingredients required to have the (transverse-isotropic) axion response are the glide-rotation symmetry and an offset angle $\theta = 45°$ between the optical axes of the permittivity and permeability. In particular, a nontrivial axion response requires permittivity and permeability tensors with an anisotropic response in the x-o-y plane.

III. THE SYNTHETIC AXION MEDIUM

Next, we investigate in detail the properties of the synthetic axion medium. Thus, in the rest of the paper the offset angle is fixed at $\theta = 45°$. In such a case, the effective medium [Eq. (15)] describes a uniaxial axion material such that $\overline{\bar{\xi}}_{ef} = \overline{\bar{\zeta}}_{ef,\perp} = \kappa_{ef}(\hat{\mathbf{x}} \otimes \hat{\mathbf{x}} + \hat{\mathbf{y}} \otimes \hat{\mathbf{y}})$.

In practice, a time-varying anisotropic permittivity can be implemented using an array of dipoles loaded with varactors, analogous to Ref. [51]. In our case, each unit cell should contain two dipoles, let us say aligned along the x
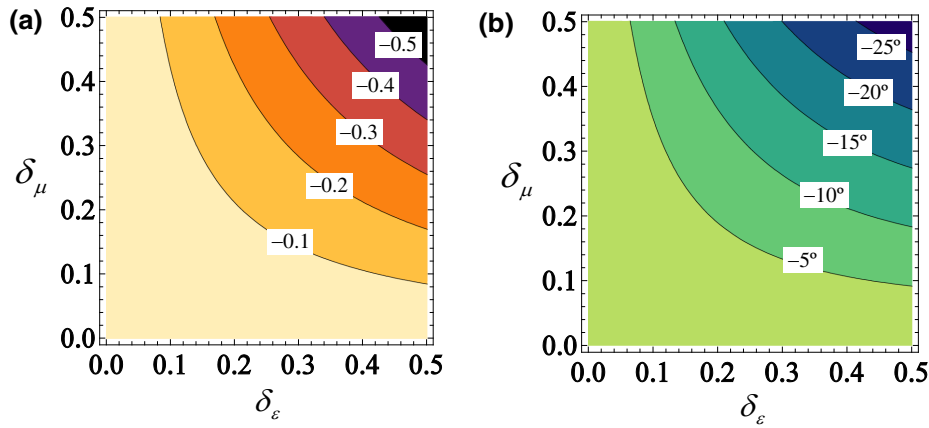
FIG. 4.   (a) Density plot of the axion parameter κ_{ef} as a function of $\delta_\varepsilon, \delta_\mu$. (b) Angle of rotation θ_R as a function of $\delta_\varepsilon, \delta_\mu$. In both plots, $\varepsilon_M = 4$ and $\mu_M = 2$ and $v/c = 0.2$.

and y directions. By changing the capacitance of the varactors in time, the polarizability of the dipoles also changes in time, so that the permittivity of the material may be assumed of the form $\bar{\varepsilon} = \mathbf{1} + \chi_{xx}(t)\hat{\mathbf{x}} \otimes \hat{\mathbf{x}} + \chi_{yy}(t)\hat{\mathbf{y}} \otimes \hat{\mathbf{y}}$. Note that the permittivity optical axes are fixed, only the eigenvalues change in time. For the magnetic permeability, we need a similar strategy (using magnetic dipoles instead of electric dipoles), but the optical axes of the permeability should be rotated by 45° with respect to the optical axes of the permittivity.

It is convenient to write the eigenvalues of the permittivity and permeability tensors, $\varepsilon_1, \varepsilon_2$ and μ_1, μ_2, of layer A as follows:

$$\varepsilon_1 = \varepsilon_M(1 + \delta_\varepsilon), \quad \varepsilon_2 = \varepsilon_M(1 - \delta_\varepsilon)$$
$$\mu_1 = \mu_M(1 + \delta_\mu), \quad \mu_2 = \mu_M(1 - \delta_\mu). \tag{19}$$

The parameters $\delta_\varepsilon, \delta_\mu$ determine the strength of the anisotropy of the electric and magnetic responses, respectively. The effective material parameters of the synthetic axion medium [Eq. (18) with $\theta = 45°$] can be written as

$$\varepsilon_{\mathrm{ef},\perp} = \varepsilon_M \frac{1 + \varepsilon_M \mu_M v^2(\delta_\varepsilon^2 - 1)}{1 - \varepsilon_M \mu_M v^2},$$
$$\mu_{\mathrm{ef},\perp} = \mu_M \frac{1 + \varepsilon_M \mu_M v^2(\delta_\mu^2 - 1)}{1 - \varepsilon_M \mu_M v^2}, \tag{20}$$
$$\kappa_{ef} = -\delta_\varepsilon \delta_\mu \frac{\varepsilon_M \mu_M v}{1 - \varepsilon_M \mu_M v^2}.$$

Equation (20) confirms that a nontrivial axion response requires that both the permittivity and permeability are anisotropic, i.e., $\delta_\varepsilon \neq 0$ and $\delta_\mu \neq 0$. If either $\delta_\varepsilon = 0$ or $\delta_\mu = 0$, the effective response becomes reciprocal. Note that when $\delta_\varepsilon = 0$ the permittivity of the two-phase crystal is uniform (i.e., there is no space-time modulation of the permittivity) due to the assumed glide-rotation symmetry.

It is relevant to underline that even though the refractive index of the effective axion medium is polarization independent, each of the material phases is birefringent and reciprocal when on its own. Specifically, in the absence of time modulations, the velocity of the wave in layer A for propagation along the $+z$ direction depends on the polarization. The wave velocities for the two eigenpolarizations in material A are (the same result is obtained for layer B):

$$\frac{v_\pm^{\mathrm{aniso}}}{c} = \frac{1}{\sqrt{\varepsilon_M \mu_M}\sqrt{1 \pm \sqrt{\delta_u^2 + \delta_\varepsilon^2 - \delta_\varepsilon^2 \delta_u^2}}}. \tag{21}$$

Thus, the subluminal range for the space-time modulation is determined by

$$0 < |v| < v_+^{\mathrm{aniso}}, \ (\text{subluminal range}). \tag{22}$$

On the other hand, the superluminal range is defined by the interval $|v| > v_-^{\mathrm{aniso}}$. In this work, we focus on the subluminal regime wherein the space-time crystal response is bounded and free of instabilities (there are no exponentially growing in time natural modes).

Equation (20) shows that the axion κ_{ef} parameter is proportional to both δ_ε and δ_μ, which determine both the anisotropy and the modulation strength. Thus, $|\kappa_{ef}|$ increases always with $|\delta_\varepsilon|$ and $|\delta_\mu|$. This property is illustrated in Fig. 4(a), for $\varepsilon_M = 4$ and $\mu_M = 2$ and for a fixed modulation speed $v/c = 0.2$. For the range of δ_ε and δ_μ in the plot, the space-time crystal is always operated in the subluminal regime. For large δ_ε and δ_μ, the subluminal threshold (v_+^{aniso}) approaches the modulation speed ($v/c = 0.2$), and the axion response is greatly enhanced. For example, for $\delta_\varepsilon = \delta_\mu = 0.5$ the effective medium has a giant nonreciprocal axion response with $\kappa_{ef} \approx -0.59$. The corresponding effective (transverse) permittivity and permeability are $\varepsilon_{\mathrm{ef},\perp} \approx 4.47$ and $\mu_{\mathrm{ef},\perp} \approx 2.24$, respectively.
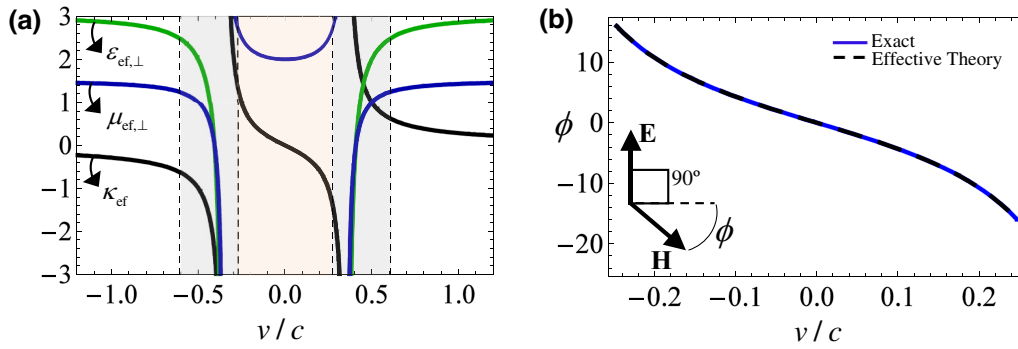
FIG. 5.   (a) Effective parameters of the synthetic axion medium as a function of the normalized modulation speed. The dashed lines mark transitions between the subluminal range (pink-shaded region), the transluminal range (gray-shaded regions) and the superluminal range (unshaded regions). (b) Offset angle ϕ between the magnetic and electric fields (see the inset) in the synthetic axion medium as a function of the modulation speed v. In both plots, $\varepsilon_M = 4$, $\mu_M = 2$ and $\delta_\varepsilon = \delta_\mu = 0.5$.

Figure 5(a) shows the effective parameters of the synthetic axion medium as a function of the modulation speed v. As seen, for a nontrivial modulation speed the axion parameter becomes nonzero. Even for very moderate modulation speeds the axion parameter can be several orders of magnitude larger than what is observed in any natural material. In the subluminal range (pink shaded region), the sign of the axion parameter is locked to the sign of the modulation speed. The axion parameter flips sign in the transluminal region ($v_+^{\text{aniso}} < |v| < v_-^{\text{aniso}}$).

In agreement with Fig. 3(a), the effective refractive index seen by a wave propagating in the synthetic axion medium is independent of the wave polarization and of the propagation ($+z$ or $-z$) direction: $n_{\text{ef}} = \sqrt{\varepsilon_{\text{ef},\perp}\mu_{\text{ef},\perp} - \kappa_{\text{ef}}^2}$. One of the peculiar properties of the effective isotropic axion response is that the (instantaneous) electric and magnetic fields are not orthogonal, different from conventional dielectrics [8]. The offset angle ϕ with respect to 90° [see the inset of Fig. 5(b)] is given by

$$\phi = \arcsin\left(\frac{\kappa_{\text{ef}}}{\sqrt{\varepsilon_{\text{ef},\perp}\,\mu_{\text{ef},\perp}}}\right). \qquad (23)$$

Figure 5(b) depicts ϕ as a function of the modulation speed for the same structural parameters as before. As seen, for a velocity near the subluminal threshold ($v/c = 0.2$) the offset angle can be as large as $\phi \approx -11°$. The effective medium prediction of ϕ agrees very precisely with the calculation of ϕ based on the spatial averaging of the long-wavelength Bloch mode fields of the space-time crystal. The Bloch modes are numerically determined as explained in Appendix C.

Furthermore, as shown in Fig. 3(c), there is an excellent agreement between the effective refractive index n_{ef} calculated with the homogenization theory (dashed line) and the refractive index extracted from the slope of the space-time crystal dispersion in the lab frame in the long wavelength limit (solid line). This is further illustrated in Fig. 6(a), which depicts the exact band diagram of the space-time crystal for $v/c = 0.2$. The dashed lines represent the dispersion predicted by homogenization theory and match precisely the exact band structure for $\omega a/c \ll 1$, where a is the lattice period. As previously mentioned, the slopes are symmetric in respect to k_z, i.e., $\omega(k_z) = \omega(-k_z)$, due to the isotropic response of the axion material. It should be noted that away from the long wavelength limit the
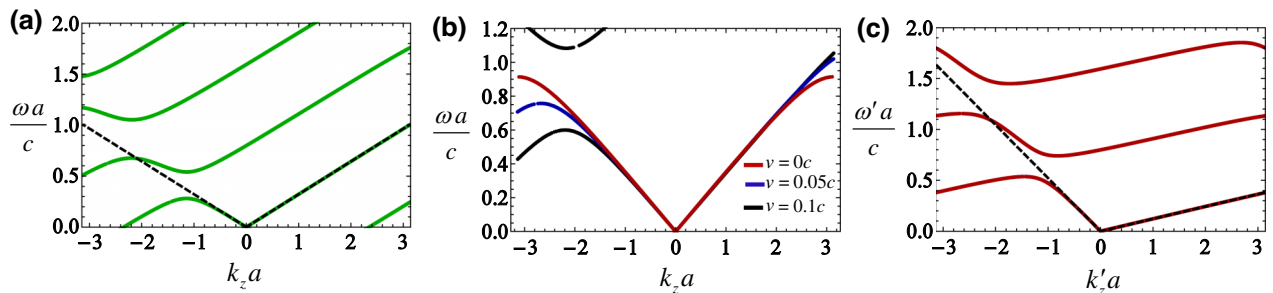

FIG. 6.   (a) Band diagram in the laboratory frame of a space-time crystal with the parameters $\varepsilon_M = 4$, $\mu_M = 2$, $\delta_\varepsilon = \delta_\mu = 0.5$ and $v/c = 0.2$. (b) Evolution of the band diagram in laboratory frame for the same material parameters as in (a) and different modulations speeds. (c) Similar to (a) but calculated in the Galilean co-moving frame. The dashed black lines in (a),(c) represent the effective medium dispersion.
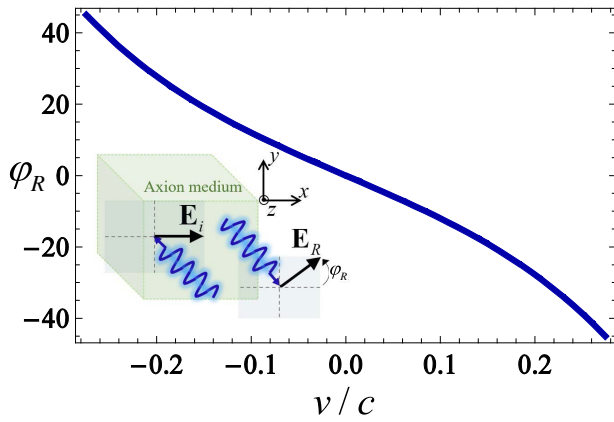
FIG. 7. Angle of polarization rotation φ_R for an air-synthetic axion medium interface, as a function of the modulation speed v. The parameters of the space-time crystal are $\varepsilon_M = 4$, $\mu_M = 2$, and $\delta_\varepsilon = \delta_\mu = 0.5$. The angle φ_R determines the rotation of the reflected field with respect to the incident linearly polarized electric field.

condition $\omega(k_z) = \omega(-k_z)$ is violated and the nonreciprocity of the space-time crystal is evident in the band diagram. Figure 6(b) shows the evolution of the band diagram as the velocity is increased from $v = 0$ (red lines) up to $v/c = 0.2$ (green lines). As seen, a larger v results in a more pronounced spectral asymmetry and in the increase of the density of states at low frequencies. For completeness, we also show the dispersion band diagram of the space-time crystal in the Galilean co-moving frame [Fig. 6(c)]. In the co-moving frame, the wave dispersion is asymmetric with respect to k_z even in the long wavelength limit.

In order to illustrate how the axion coupling can tailor the light-matter interactions in the space-time crystal, we consider a simple scattering problem, where a normally incident linearly polarized plane wave propagating in air $(z < 0)$ illuminates the synthetic axion medium $(z > 0)$ (see the inset of Fig. 7). The wave scattering is characterized using the effective medium model.

As is well known [8], under the described conditions the reflected wave is also linearly polarized, but the electric field of the reflected wave is rotated by some angle φ_R with respect to the incident field. The rotation of polarization of the reflected wave is a clear fingerprint of the axion response, and it is only possible due the nonreciprocity of the effective medium.

For an air-axion material interface the polarization rotation angle is given by [8]

$$\varphi_R = \arctan\left(\frac{2\kappa_{\text{ef}}}{\varepsilon_{\text{ef},\perp} - \mu_{\text{ef},\perp}}\right). \qquad (24)$$

It can be shown that φ_R is independent of the axion-material slab thickness. Note that when $\varepsilon_{\text{ef},\perp} = \mu_{\text{ef},\perp}$ the angle is not defined because in that case the reflection coefficient vanishes (not shown). Figure 7 depicts the rotation

angle φ_R as a function of the modulation speed v. When $v/c = 0.2$ the angle can be as large as $\varphi_R \approx -27.76°$, resulting in a strongly nonreciprocal scattering rooted in the synthetic axion response.

The angle of rotation φ_R may be written explicitly in terms of $\varepsilon_M, \mu_M, \delta_\varepsilon, \delta_\mu$ [Eq. (20)] as

$$\varphi_R = \arctan$$

$$\left(\frac{-2\delta_\varepsilon \delta_\mu \varepsilon_M \mu_M v}{\varepsilon_M - \mu_M + \varepsilon_M \mu_M v^2 [\mu_M(1 - \delta_\mu^2) - \varepsilon_M(1 - \delta_\varepsilon^2)]}\right). \qquad (25)$$

A density plot of φ_R as a function of δ_ε, δ_μ is shown in Fig. 4(b). Similar to the axion parameter, the magnitude of φ_R increases monotonically with $|\delta_\varepsilon|$ and $|\delta_\mu|$. In the absence of a space-time modulation, i.e., for $|\delta_\varepsilon| = |\delta_\mu| = 0$, the effective response is reciprocal and the axion parameter vanishes [Fig. 4(a)]; accordingly, in this case the angle of rotation also vanishes, $\varphi_R = 0$. For completeness, we point out that the combination of a chiral response with an axion-type response can be used to design one-way devices and optical isolators [12].

IV. CONCLUSIONS

In summary, it was demonstrated that space-time modulations provide an exciting path to sculpt the nonreciprocal response in the long wavelength limit. In particular, the type of anisotropy of the underlying photonic crystal (without time modulation) determines the symmetry of the effective magnetoelectric tensor of the metamaterial. While for isotropic materials the effective response reduces always to that of a moving medium, crystals made of anisotropic materials offer increased design flexibility and, in particular, may allow probing rather unique nonreciprocal couplings. Here, it is shown that when the space-time crystal has glide-rotation symmetry its effective response in the *x-o-y* plane becomes independent of the wave polarization, and the effective material behaves as uniaxial moving-Tellegen medium. The relative strength of the axion and moving medium effective parameters depends on the angle θ between the optical axes of the permittivity and permeability tensors. It is shown that for a two-phase space-time crystal an offset angle $\theta = 45°$ results in an ideal (uniaxial) synthetic axion response in the long wavelength limit. The synthetic axion-coupling enables a giant nonreciprocal polarization rotation in reflection mode, which can be exploited to realize nonreciprocal mirrors and related devices. Hence, our work unveils a different physical mechanism and an exciting opportunity to implement the elusive Tellegen-medium response using space-time modulations. It is envisioned that systems with a synthetic axion coupling may offer unique opportunities to sculpt and control nonreciprocal light-matter interactions.

APPENDIX A: MATERIAL MATRIX TRANSFORMATION

A Lorentz transformation of coordinates preserves the structure of Maxwell's equations provided the fields are transformed as (the primed frame moves with speed $\mathbf{v}$ with respect to the lab frame; $\gamma = 1/\sqrt{1 - v^2/c^2}$ is the Lorentz factor) [52]

$$\mathbf{E}'_{||} = \mathbf{E}_{||}, \quad \mathbf{B}'_{||} = \mathbf{B}_{||}, \tag{A1a}$$

$$\mathbf{E}'_\perp = \gamma(\mathbf{E}_\perp + \mathbf{v} \times \mathbf{B}), \quad \mathbf{B}'_\perp = \gamma\left(\mathbf{B}_\perp - \frac{1}{c^2}\mathbf{v} \times \mathbf{E}\right), \tag{A1b}$$

and

$$\mathbf{D}'_{||} = \mathbf{D}_{||}, \quad \mathbf{H}'_{||} = \mathbf{H}_{||}, \tag{A2a}$$

$$\mathbf{D}'_\perp = \gamma\left(\mathbf{D}_\perp + \frac{1}{c^2}\mathbf{v} \times \mathbf{H}\right), \quad \mathbf{H}'_\perp = \gamma(\mathbf{H}_\perp - \mathbf{v} \times \mathbf{D}). \tag{A2b}$$

Here $||$ and $\perp$ represent the field components parallel and perpendicular to the velocity. The same relations can be written in vector notation as

$$\begin{pmatrix}\mathbf{E}' \\ \mathbf{H}'\end{pmatrix} = \underbrace{\begin{pmatrix}\gamma\mathbf{1}_\perp + \hat{\mathbf{u}}_{||} \otimes \hat{\mathbf{u}}_{||} & \mathbf{0} \\ \mathbf{0} & \gamma\mathbf{1}_\perp + \hat{\mathbf{u}}_{||} \otimes \hat{\mathbf{u}}_{||}\end{pmatrix}}_{\mathbf{A}}\begin{pmatrix}\mathbf{E} \\ \mathbf{H}\end{pmatrix}$$

$$+ \underbrace{\begin{pmatrix}\mathbf{0} & \gamma\mathbf{v} \times \mathbf{1} \\ -\gamma\mathbf{v} \times \mathbf{1} & \mathbf{0}\end{pmatrix}}_{\mathbf{V}}\begin{pmatrix}\mathbf{D} \\ \mathbf{B}\end{pmatrix} \tag{A3a}$$

$$\begin{pmatrix}\mathbf{D}' \\ \mathbf{B}'\end{pmatrix} = \frac{1}{c^2}\underbrace{\begin{pmatrix}\mathbf{0} & \gamma\mathbf{v} \times \mathbf{1} \\ -\gamma\mathbf{v} \times \mathbf{1} & \mathbf{0}\end{pmatrix}}_{\mathbf{V}}\begin{pmatrix}\mathbf{E} \\ \mathbf{H}\end{pmatrix}$$

$$+ \underbrace{\begin{pmatrix}\gamma\mathbf{1}_\perp + \hat{\mathbf{u}}_{||} \otimes \hat{\mathbf{u}}_{||} & \mathbf{0} \\ \mathbf{0} & \gamma\mathbf{1}_\perp + \hat{\mathbf{u}}_{||} \otimes \hat{\mathbf{u}}_{||}\end{pmatrix}}_{\mathbf{A}}\begin{pmatrix}\mathbf{D} \\ \mathbf{B}\end{pmatrix} \tag{A3b}$$

with $\mathbf{1}_\perp = \mathbf{1} - \hat{\mathbf{u}}_{||} \otimes \hat{\mathbf{u}}_{||}$.

Suppose now that in the lab frame,

$$\begin{pmatrix}\mathbf{D}(x,y,z,t) \\ \mathbf{B}(x,y,z,t)\end{pmatrix} = \mathbf{M}(x,y,z,t) \cdot \begin{pmatrix}\mathbf{E}(x,y,z,t) \\ \mathbf{H}(x,y,z,t)\end{pmatrix}. \tag{A4}$$

Then, from Eq. (A3) it follows that in the co-moving frame:

$$\begin{pmatrix}\mathbf{E}' \\ \mathbf{H}'\end{pmatrix} = [\mathbf{A} + \mathbf{V} \cdot \mathbf{M}(x',y',z',t')] \cdot \begin{pmatrix}\mathbf{E} \\ \mathbf{H}\end{pmatrix},$$

$$\begin{pmatrix}\mathbf{D}' \\ \mathbf{B}'\end{pmatrix} = \left[\frac{1}{c^2}\mathbf{V} + \mathbf{A} \cdot \mathbf{M}(x',y',z',t')\right] \cdot \begin{pmatrix}\mathbf{E} \\ \mathbf{H}\end{pmatrix}. \tag{A5}$$

Hence, the constitutive relations in the co-moving frame are

$$\begin{pmatrix}\mathbf{D}' \\ \mathbf{B}'\end{pmatrix} = \left[\frac{1}{c^2}\mathbf{V} + \mathbf{A} \cdot \mathbf{M}\right] \cdot [\mathbf{A} + \mathbf{V} \cdot \mathbf{M}]^{-1} \cdot \begin{pmatrix}\mathbf{E}' \\ \mathbf{H}'\end{pmatrix}. \tag{A6}$$

So that the equivalent material matrix is given by

$$\mathbf{M}' = \left[\frac{1}{c^2}\mathbf{V} + \mathbf{A} \cdot \mathbf{M}\right] \cdot [\mathbf{A} + \mathbf{V} \cdot \mathbf{M}]^{-1}. \tag{A7}$$

In the Lorentz transformation the parameter "c" can be regarded as a free parameter not necessarily linked to the speed of light in vacuum $1/\sqrt{\varepsilon_0\mu_0}$. The standard Lorentz transformation with $c = 1/\sqrt{\varepsilon_0\mu_0}$ simply ensures that the vacuum response stays invariant under the coordinate transformation.

The case of Galilean transformation corresponds to taking the limit $c \to \infty$. In this limit, $\mathbf{A} = \mathbf{1}, \mathbf{V} = \begin{pmatrix}0 & \mathbf{v} \times \mathbf{1} \\ -\mathbf{v} \times \mathbf{1} & 0\end{pmatrix}$, and thereby,

$$\mathbf{M}' = \mathbf{M} \cdot [\mathbf{1} + \mathbf{V} \cdot \mathbf{M}]^{-1}. \tag{A8}$$

It can be shown (details omitted for conciseness) that the effective material response in the lab frame obtained using a Galilean transformation is exactly the same as the response obtained with the Lorentz transformation.

Let us now suppose that the permittivity and permeability tensors in the laboratory frame have the structure shown in Eq. (3). Then, $\mathbf{M}'$ determined by Eq. (A8) is of the form

$$\mathbf{M}' = \begin{pmatrix}\varepsilon_0\bar{\varepsilon}' & \frac{1}{c}\overline{\xi}' \\ \frac{1}{c}\overline{\zeta}' & \mu_0\overline{\mu}'\end{pmatrix}, \text{ with} \tag{A9a}$$

$$\bar{\varepsilon}' = \begin{pmatrix}\varepsilon'_{xx} & \varepsilon'_{xy} & 0 \\ \varepsilon'_{xy} & \varepsilon'_{yy} & 0 \\ 0 & 0 & \varepsilon_{zz}\end{pmatrix}, \quad \overline{\mu}' = \begin{pmatrix}\mu'_{xx} & \mu'_{xy} & 0 \\ \mu'_{xy} & \mu'_{yy} & 0 \\ 0 & 0 & \mu_{zz}\end{pmatrix}, \tag{A9b}$$

$$\overline{\xi}' = \overline{\zeta}'^T = \begin{pmatrix}\xi'_{xx} & \xi'_{xy} & 0 \\ \xi'_{yx} & \xi'_{yy} & 0 \\ 0 & 0 & 0\end{pmatrix} \tag{A9c}$$

Note that $\mathbf{M}'$ is a symmetric real-valued matrix and thereby is diagonalizable. Clearly, two of the eigenvectors of $\mathbf{M}'$

are of the type $(\hat{\mathbf{z}} \quad 0)^T$ and $(0 \quad \hat{\mathbf{z}})^T$. The other four eigenvectors are of the type $(\mathbf{u}_E \quad \mathbf{u}_H)^T$ with $\mathbf{u}_E, \mathbf{u}_H$ some vectors in the x-o-y plane, i.e., perpendicular to the direction of the modulation speed. This means that the response of the crystal along the z' direction (parallel to the modulation speed) is effectively decoupled from the response of the material in the x-o-y plane.

APPENDIX B: HOMOGENIZATION IN THE LONG WAVELENGTH LIMIT

The effective medium theory links the spatially averaged fields in the co-moving frame as

$$
\begin{pmatrix} \langle \mathbf{D}' \rangle \\ \langle \mathbf{B}' \rangle \end{pmatrix} = \mathbf{M}'_{\text{ef}} \cdot \begin{pmatrix} \langle \mathbf{E}' \rangle \\ \langle \mathbf{H}' \rangle \end{pmatrix}. \tag{B1}
$$

Here, $\langle \ldots \rangle$ denotes the operation of spatial averaging. For a periodic structure the averaging is defined as

$$
\langle f \rangle = \frac{1}{a} \int_0^a dz' \, f(z'), \tag{B2a}
$$

with a the lattice constant. As is well known, due to the structure of Maxwell's equations, for stratified systems such that $\mathbf{M}' = \mathbf{M}'(z')$ the tangential field components $\mathbf{E}, \mathbf{H}$, i.e., E'_x, E'_y, H'_x, H'_y, can be assumed constant in the long wavelength limit ($i\partial_{t'} = \omega' \to 0$). This means that

$$
E'_x = \langle E'_x \rangle, \quad E'_y = \langle E'_y \rangle, \quad H'_x = \langle H'_x \rangle, \quad H'_y = \langle H'_y \rangle. \tag{B3a}
$$

Similarly, the normal components of the fields $\mathbf{D}, \mathbf{B}$ are also constant in the long wavelength limit:

$$
D'_z = \langle D'_z \rangle, \quad B'_z = \langle B'_z \rangle. \tag{B3b}
$$

Taking into account that the microscopic fields are linked by $\begin{pmatrix} \mathbf{D}' \\ \mathbf{B}' \end{pmatrix} = \mathbf{M}'(z') \cdot \begin{pmatrix} \mathbf{E}' \\ \mathbf{H}' \end{pmatrix}$ with $\mathbf{M}'(z') = \mathbf{M} \cdot [\mathbf{1} + \mathbf{V} \cdot \mathbf{M}]^{-1}$ having the structure shown in Eq. (A9), it is clear from Eq. (B3) that the effective material response is of the type:

$$
\mathbf{M}'_{\text{ef}} = \begin{pmatrix} \varepsilon_0 \overline{\varepsilon'_{\text{ef}}} & \frac{1}{c}\overline{\xi'_{\text{ef}}} \\ \frac{1}{c}\overline{\zeta'_{\text{ef}}} & \mu_0 \overline{\mu'_{\text{ef}}} \end{pmatrix}, \text{ with} \tag{B4a}
$$

$$
\overline{\varepsilon'_{\text{ef}}} = \begin{pmatrix} \langle \varepsilon'_{xx} \rangle & \langle \varepsilon'_{xy} \rangle & 0 \\ \langle \varepsilon'_{xy} \rangle & \langle \varepsilon'_{yy} \rangle & 0 \\ 0 & 0 & \frac{1}{\langle 1/\varepsilon_{zz} \rangle} \end{pmatrix},
$$

$$
\overline{\mu'_{\text{ef}}} = \begin{pmatrix} \langle \mu'_{xx} \rangle & \langle \mu'_{xy} \rangle & 0 \\ \langle \mu'_{xy} \rangle & \langle \mu'_{xx} \rangle & 0 \\ 0 & 0 & \frac{1}{\langle 1/\mu_{zz} \rangle} \end{pmatrix}, \tag{B4b}
$$

$$
\overline{\xi'_{\text{ef}}} = \overline{\zeta'_{\text{ef}}}^T = \begin{pmatrix} \langle \xi'_{xx} \rangle & \langle \xi'_{xy} \rangle & 0 \\ \langle \xi'_{yx} \rangle & \langle \xi'_{yy} \rangle & 0 \\ 0 & 0 & 0 \end{pmatrix}. \tag{B4c}
$$

Note that the material parameters that determine the response in the x-o-y plane are simply averaged in space, whereas the material parameters in the direction of the modulation speed (z) are determined by the average of the inverse function.

The effective response in the lab frame can be found with an inverse Galilean transformation [compare with Eq. (A8)]:

$$
\mathbf{M}_{\text{ef}} = \mathbf{M}'_{\text{ef}} \cdot [\mathbf{1} - \mathbf{V} \cdot \mathbf{M}'_{\text{ef}}]^{-1}. \tag{B5}
$$

It can be easily shown that the inverse Galilean transformation preserves the structure shown in Eq. (B4), so that one obtains Eq. (7) of the main text.

APPENDIX C: BAND STRUCTURE OF THE SPACE-TIME CRYSTAL

In this Appendix, we explain how the exact band structure of the space-time crystal is calculated. For simplicity, we restrict our attention to waves propagating along the z direction, i.e., along the direction of the modulation speed. In that case, Maxwell's equations in the Galilean co-moving frame can be written as

$$
i\frac{d}{dz'}\boldsymbol{\sigma} \cdot \begin{pmatrix} \mathbf{E}'_\perp \\ \mathbf{H}'_\perp \end{pmatrix} = i\frac{\partial}{\partial t'}\left[\mathbf{M}'_\perp(z') \cdot \begin{pmatrix} \mathbf{E}'_\perp \\ \mathbf{H}'_\perp \end{pmatrix} \right], \tag{C1a}
$$

$$
\mathbf{M}'_\perp(z') = \mathbf{M}_\perp(z') \cdot [\mathbf{1}_{4 \times 4} + v\boldsymbol{\sigma} \cdot \mathbf{M}_\perp(z')]^{-1}. \tag{C1b}
$$

In the above $\boldsymbol{\sigma}$ is defined as in Eq. (10), $\mathbf{M}_\perp(z')$ is given by Eq. (4), and $\mathbf{E}'_\perp = (E'_x \quad E'_y)^T$ and $\mathbf{H}'_\perp = (H'_x \quad H'_y)^T$ are the transverse fields in the co-moving frame. It should be noted that $\mathbf{M}'_\perp(z')$ is formed by the elements of $\mathbf{M}'(z')$ [Eq. (A8)] that determine the response of the crystal to a transverse excitation.

Let us find the Bloch mode solutions of Eq. (C1) with $i(\partial/\partial t') = \omega'$ the oscillation frequency and k_z' the Bloch wave number in the Galilean co-moving frame. We consider the case of a two-phase space-time crystal [Fig. 1]. In each homogeneous region of space, Eq. (C1) is equivalent to $(d/dz')\begin{pmatrix}\mathbf{E}_\perp' \\ \mathbf{H}_\perp'\end{pmatrix} = -i\omega'\boldsymbol{\sigma}\cdot\mathbf{M}_\perp'\cdot\begin{pmatrix}\mathbf{E}_\perp' \\ \mathbf{H}_\perp'\end{pmatrix}$. It was taken into account that $\boldsymbol{\sigma}^2 = \mathbf{1}_{4\times 4}$. This equation can be formally integrated as

$$\begin{pmatrix}\mathbf{E}_\perp'(z') \\ \mathbf{H}_\perp'(z')\end{pmatrix} = \exp\left(-i\omega'(z'-z_0')\boldsymbol{\sigma}\cdot\mathbf{M}_\perp'\right)\cdot\begin{pmatrix}\mathbf{E}_\perp'(z_0') \\ \mathbf{H}_\perp'(z_0')\end{pmatrix}, \tag{C2a}$$

where $\exp(\ldots)$ stands for the exponential of a matrix. Hence, for a two-phase crystal with layers A and B of identical thickness (half-lattice constant, $a/2$) one can write

$$\begin{pmatrix}\mathbf{E}_\perp'(z_0'+a) \\ \mathbf{H}_\perp'(z_0'+a)\end{pmatrix}$$
$$= \exp\left(-i\frac{\omega'a}{2}\boldsymbol{\sigma}\cdot\mathbf{M}_{\perp,\mathrm{B}}'\right)\cdot\exp\left(-i\frac{\omega'a}{2}\boldsymbol{\sigma}\cdot\mathbf{M}_{\perp,\mathrm{A}}'\right)$$
$$\cdot\begin{pmatrix}\mathbf{E}_\perp'(z_0') \\ \mathbf{H}_\perp'(z_0')\end{pmatrix}. \tag{C3}$$

Here, $\mathbf{M}_{\perp,i}'$ is the (transverse) material matrix for layer $i = A, B$. Imposing the Bloch mode condition, $\begin{pmatrix}\mathbf{E}_\perp'(z_0'+a) \\ \mathbf{H}_\perp'(z_0'+a)\end{pmatrix} = e^{ik_z'a}\begin{pmatrix}\mathbf{E}_\perp'(z_0') \\ \mathbf{H}_\perp'(z_0')\end{pmatrix}$, one obtains the secular equation:

$$\det\left(\exp\left(-i\frac{\omega'a}{2}\boldsymbol{\sigma}\cdot\mathbf{M}_{\perp,\mathrm{B}}'\right)\cdot\exp\left(-i\frac{\omega'a}{2}\boldsymbol{\sigma}\cdot\mathbf{M}_{\perp,\mathrm{A}}'\right)\right.$$
$$\left.-e^{ik_z'a}\mathbf{1}_{4\times 4}\right) = 0, \tag{C4}$$

whose solutions determine the dispersion ω' vs. k_z' of the crystal in the Galilean co-moving frame. Note that for a fixed ω', the solutions for k_z' are such that $e^{ik_z'a}$ is an eigenvalue of the matrix $\exp\left(-i(\omega'a/2)\boldsymbol{\sigma}\cdot\mathbf{M}_{\perp,\mathrm{B}}'\right)\cdot\exp\left(-i(\omega'a/2)\boldsymbol{\sigma}\cdot\mathbf{M}_{\perp,\mathrm{A}}'\right)$. The dispersion in the lab frame ω vs. k_z can be found from the dispersion in the co-moving frame using $\omega = \omega' + k_z'v$ and $k_z = k_z'$.

---

[1] D. R. Smith, Willie J. Padilla, D. C. Vier, S. C. Nemat-Nasser, and S. Schultz, Composite Medium with Simultaneously Negative Permeability and Permittivity, Phys. Rev. Lett. **84**, 4184 (2000).

[2] P. A. Belov, Y. Hao, and S. Sudhakaran, Subwavelength microwave imaging using an array of parallel conducting wires as a lens, Phys. Rev. B **73**, 033108 (2006).

[3] A. Salandrino and N. Engheta, Far-field subdiffraction optical microscopy using metamaterial crystals: Theory and simulations, Phys. Rev. B **74**, 075103 (2006).

[4] Z. Jacob, L. V. Alekseyev, and E. Narimanov, Optical hyperlens: far-field imaging beyond the diffraction limit, Opt. Express **14**, 8247 (2006).

[5] A. B. Khanikaev, S. H. Mousavi, W. K. Tse, M. Kargarian, A. H. MacDonald, and G. Shvets, Photonic topological insulators, Nat. Mater. **12**, 233 (2012).

[6] W.-J. Chen, Z.-Q. Zhang, J.-W. Dong, and C. T. Chan, Symmetry-protected transport in a pseudospinpolarized waveguide, Nat. Commun. **6**, 8183 (2015).

[7] M. G. Silveirinha, PTD symmetry protected scattering anomaly in optics, Phys. Rev. B **95**, 035153 (2017).

[8] I. V. Lindell, A. H. Sihvola, S. A. Tretyakov, and A. J. Viitanen, *Electromagnetic Waves in Chiral and Bi-Isotropic Media. Boston* (Artech House, MA, 1994).

[9] F. R. Prudêncio, S. A. Matos, and C. R. Paiva, A geometrical approach to duality transformations for Tellegen media, IEEE Trans. Microwave Theory Tech. **62**, 1417 (2014).

[10] F. Prudêncio, S. A. Matos, and C. R. Paiva, Asymmetric band diagrams in photonic crystals with a spontaneous nonreciprocal response, Phys. Rev. A **91**, 063821 (2015).

[11] P. W. Anderson, More is different, Science **177**, 393 (1972).

[12] F. R. Prudêncio and M. G. Silveirinha, Optical isolation of circularly polarized light with a spontaneous magnetoelectric effect, Phys. Rev. A **93**, 043846 (2016).

[13] D. N. Astrov, Magnetoelectric effect in chromium oxide, Sov. Phys. JETP **13**, 729 (1961).

[14] R. S. K. Mong, A. M. Essin, and J. E. Moore, Antiferromagnetic topological insulators, Phys. Rev. B **81**, 245209 (2010).

[15] A. N. Serdyukov, A. H. Sihvola, S. A. Tretyakov, and I. V. Semchenko, Duality in electromagnetics: application to Tellegen media, Electromagnetics **16**, 51 (1996).

[16] A. Lakhtakia and W. S. Weiglhofer, Are linear, nonreciprocal, biisotropic media forbidden?, IEEE Trans. Microwave Theory Tech. **42**, 1715 (1994).

[17] A. H. Sihvola, Are nonreciprocal bi-isotropic media forbidden indeed?, IEEE Trans. Microwave Theory Tech. **43**, 2160 (1995).

[18] A. Lakhtakia and W. S. Weiglhofer, Comment on "Are nonreciprocal bi-isotropic media forbidden indeed?, IEEE Trans. Microwave Theory Tech. **43**, 2722 (1995).

[19] A. H. Sihvola, S. A. Tretyakov, A. N. Serdyukov, and I. V. Semchenko, Duality once more applied to Tellegen media, Electromagnetics **17**, 205 (1997).

[20] A. Lakhtakia and W. S. Weiglhofer, On the application of duality to Tellegen media, Electromagnetics **17**, 199 (1997).

[21] Y. N. Obukhov and F. W. Hehl, On the boundary-value problems and the validity of the Post constraint in modern electromagnetism, Optik **120**, 418 (2009).

[22] A. Lakhtakia, Remarks on the current status of the post constraint, Optik **120**, 422 (2009).

[23] V. Dziom, A. Shuvaev, A. Pimenov, G. V. Astakhov, C. Ames, K. Bendias, J. Böttcher, G. Tkachov, E. M. Hankiewicz, C. Brüne, H. Buhmann and L. W. Molenkamp, Observation of the universal magnetoelectric effect in a 3D topological insulator, Nat. Commun. **8**, 15197 (2017).

[24] X.-L. Qi, R. Li, J. Zang, and S.-C. Zhang, Inducing a magnetic monopole with topological surface states, Science **323**, 1184 (2009).

[25] A. Sekine and K. Nomura, Axion electrodynamics in topological materials, J. Appl. Phys. **129**, 141101 (2021).

[26] J. Preskill, M. B. Wise, and F. Wilczek, Cosmology of the invisible axion, Phys. Lett. B **120**, 127 (1983).

[27] S. A. Tretyakov, S. I. Maslovski, I. S. Nefedov, A. J. Viitanen, P. A. Belov, and A. Sanmartin, Artificial Tellegen particle, Electromagnetics **23**, 665 (2003).

[28] T. Kodera, D. L. Sounas, and C. Caloz, Artificial Faraday rotation using a ring metamaterial structure without static magnetic field, Appl. Phys. Lett. **99**, 031114 (2011).

[29] Y. Ra'di and A. Grbic, Magnet-free nonreciprocal bianisotropic metasurfaces, Phys. Rev. B **94**, 195432 (2016).

[30] E. Galiffi, R. Tirole, S. Yin, H. Li, S. Vezzoli, P. A. Huidrobo, M. G. Silveirinha, R. Sapienza, A. Alù, and J. B. Pendry, Photonics of time-varying media, Adv. Photonics **4**, 014002 (2022).

[31] F. Biancalana, A. Amann, A. V. Uskov, and E. P. O'Reilly, Dynamics of light propagation in spatiotemporal dielectric structures, Phys. Rev. E **75**, 046607 (2007).

[32] Z. Yu and S. Fan, Complete optical isolation created by indirect interband photonic transitions, Nat. Photonics **3**, 91 (2009).

[33] D. L. Sounas and A. Alù, Non-reciprocal photonics based on time modulation, Nat. Photonics **11**, 774 (2017).

[34] Z. Deck-Léger, N. Chamanara, M. Skorobogatiy, M. G. Silveirinha, and C. Caloz, Uniform-velocity spacetime crystals, Adv. Photonics **1**, 1 (2019).

[35] C. Caloz and Z. Deck-Léger, Spacetime metamaterials, Part I: General concepts, IEEE Trans. Antennas Propag. **68**, 1569 (2020).

[36] X. Wang, G. Ptitcyn, V. S. Asadchy, A. Díaz-Rubio, M. S. Mirmoosa, S. Fan, and S. A. Tretyakov, Nonreciprocity in Bianisotropic Systems with Uniform Time Modulation, Phys. Rev. Lett. **125**, 195432 (2020).

[37] X. Wang, A. Díaz-Rubio, H. Li, S. A. Tretyakov, and A. Alù, Theory and Design of Multifunctional Space-Time Metasurfaces, Phys. Rev. Appl. **13**, 044040 (2020).

[38] D. Torrent, O. Poncelet, and J.-C. Batsale, Nonreciprocal Thermal Material by Spatiotemporal Modulation, Phys. Rev. Lett. **120**, 125501 (2018).

[39] M. Camacho, B. Edwards, and N. Engheta, Achieving asymmetry and trapping in diffusion with spatiotemporal metamaterials, Nat. Commun. **11**, 3733 (2020).

[40] D. Torrent, Strong spatial dispersion in time-modulated dielectric media, Phys. Rev. B **102**, 214202 (2020).

[41] P. A. Huidobro, E. Galiffi, S. Guenneau, R. V. Craster, and J. B. Pendry, Fresnel drag in space–time-modulated metamaterials, Proc. Natl. Acad. Sci. U. S. A. **116**, 24943 (2019).

[42] E. Galiffi, P. A. Huidrobo, and J. B. Pendry, An Archimedes' screw for light, Nat. Commun. **13**, 2523 (2022).

[43] P. Huidobro, M. G. Silveirinha, E. Galiffi, and J. B. P. Pendry, Homogenization Theory of Space-Time Metamaterials, Phys. Rev. Appl. **16**, 014044-1 (2021).

[44] H. T. To, Homogenization of dynamic laminates, J. Math. Anal. Appl. **354**, 518 (2009).

[45] E. Cassedy and A. Oliner. Dispersion relations in time-space periodic media: Part I—Stable interactions, Proc. IEEE **51**, 1342 (1963).

[46] E. Cassedy, Dispersion relations in time-space periodic media part II—Unstable interactions, Proc. IEEE **55**, 1154 (1967).

[47] V. Pacheco-Peña and N. Engheta, Temporal aiming, Light: Sci. Appl. **9**, 1 (2020).

[48] V. Pacheco-Peña and N. Engheta, Spatiotemporal isotropic-to-anisotropic meta-atoms, New J. Phys. **23**, 095006 (2021).

[49] O. Quevedo-Teruel, G. Valerio, and E. Rajo-Iglesias, Periodic structures with higher symmetries: Their applications in electromagnetic devices, IEEE Microwave Mag. **21**, 36 (2020).

[50] A. N. Serdyukov, I. V. Semchenko, S. A. Tretyakov, and A. H. Sihvola, *Electromagnetics of Bi-anisotropic Materials: Theory and Applications* (Gordon and Breach Science Publishers, Amsterdam, Netherlands, 2001).

[51] M. Kreiczer and Y. Hadad, Wave Analysis and Homogenization of a Spatiotemporally Modulated Wire Medium, Phys. Rev. Appl. **16**, 054003 (2021).

[52] J. D. Jackson, *Classical Electrodynamics* (Wiley, New York, 1999).